Journal of Sound and Vibration (2001) **242**(3), 411–426
doi:10.1006/jsvi.2000.3375, available online at http://www.idealibrary.com on IDEAL®

DYNAMICS OF A THREE-DIMENSIONAL OVERHEAD CRANE SYSTEM

D. C. D. Oguamanam and J. S. Hansen

Institute for Aerospace Studies, University of Toronto, 4925 Dufferin Street, Toronto, Ontario. Canada M3H 5T6

AND

G. R. Heppler

Systems Design Engineering, University of Waterloo, Waterloo, Ontario Canada N2L 3G1

(*Received* 2 *March* 2000, *and in final form* 16 *August* 2000)

An overhead crane, modelled as a point mass carriage traversing a simply supported Euler–Bernoulli beam that is allowed to travel in a direction perpendicular to its span, is considered. The point mass payload is attached to the carriage via a massless beam and is allowed both in-plane and out-of-plane motion. The Rayleigh–Ritz solution technique is used to obtain the equations of motion of the system. The influence of traverse and travel motions, pendulum length and payload mass on the pendulum motion are investigated.

1. INTRODUCTION

Overhead cranes are used in industry primarily for moving heavy payloads. The desire to move the payload in the shortest possible time is counterbalanced by the tendency of the payload swing to increase with increasing carriage acceleration. This behavior can be ameliorated with an automatic controller but to do so requires an accurate characterization of the system dynamics [1, 2]. The dynamics of elastic continua with moving loads has been covered by Fryba [3] and more recent work presents the approximate analytical solutions [4–7] and finite element solutions [8, 9] to similar problems. The interested reader can consult these and the references therein.

The assumptions made in reference [10], where the payload motion is limited to the vertical plane containing the beam, led to a system of equations where the beam dynamics were independent of the payload dynamics but not conversely. The present study extends that investigation to include in-plane and out-of-plane motion. Lee [11] implements a similar extension but ignores the beam dynamics. Here the flexibility of the beam in both directions is accounted for and the carriage can accelerate along the length of the beam (referred to as traversal) and the beam can accelerate in a direction perpendicular to its axis (referred to as travel). The beam is modelled as an Euler–Bernoulli beam, the carriage is modelled as a point mass that can traverse the beam from one end to the other, and the payload is assumed to be a point mass attached to the carriage via a massless beam (referred to together as the pendulum). The Rayleigh–Ritz solution technique is used to obtain the equations of motion of the system which are solved

0022-460X/01/180411 + 16 $35.00/0

with a modified Newmark method [8]. In the sequel, the effects of the beam travel and carriage traverse profiles, the length of the pendulum, and the payload mass on the swing of the pendulum are investigated.

2. DESCRIPTION OF THE SYSTEM

The system is depicted in Figure 1 where the payload of mass m_p is attached to the carriage via a massless beam of length L_p, the carriage has mass m_c, and the beam has length L_b. The carriage is prescribed to traverse the beam from the left-hand end to the right-hand end through a distance x_c and the beam may also have a prescribed travel in the Y-direction of y_b. An inertial frame XYZ is attached at the point O with the unit vectors $[\hat{\mathbf{a}}_1, \hat{\mathbf{a}}_2, \hat{\mathbf{a}}_3]$ defined along the X-, Y- and Z-axis respectively. The pendulum angles of swing are assumed to be small and is represented by the angles θ_x (measured from the YZ-plane) and θ_y (measured from the XZ-plane).

3. EQUATIONS OF MOTION

The position vector of an elemental mass of the beam, $\bar{\mathbf{r}}_b$, is given as

$$\bar{\mathbf{r}}_b = x\hat{\mathbf{a}}_1 + (y_b + v(x, t))\hat{\mathbf{a}}_2 + w(x, t)\hat{\mathbf{a}}_3, \tag{1}$$

The position vector of the carriage mass, $\bar{\mathbf{r}}_c$, may be expressed as

$$\bar{\mathbf{r}}_c = x_c\hat{\mathbf{a}}_1 + (y_b + v(x_c, t))\hat{\mathbf{a}}_2 + w(x_c, t)\hat{\mathbf{a}}_3, \tag{2}$$

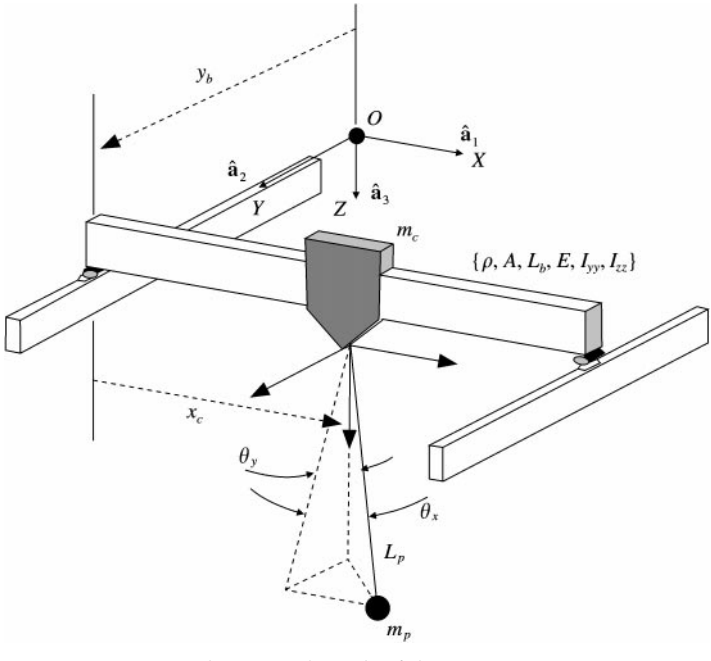

Figure 1. Schematic of the system.

and the position vector of the payload $\bar{\mathbf{r}}_p$ can be written as

$$\bar{\mathbf{r}}_p = (x_c + L_p \sin\theta_x)\hat{\mathbf{a}}_1 + (y_b + v(x_c, t) + L_p \cos\theta_x \sin\theta_y)\hat{\mathbf{a}}_2 + (w(x_c, t) + L_p \cos\theta_x \cos\theta_y)\hat{\mathbf{a}}_3. \tag{3}$$

where $w(x, t)$ and $v(x, t)$ are the in-plane (Z-direction) and the out-of-plane (Y-direction) elastic deformations of the beam.

The kinetic energy of the system $\mathscr{T}$ is composed of contributions from the beam $\mathscr{T}_b$, the carriage $\mathscr{T}_c$, and the payload $\mathscr{T}_p$. These may be expressed as

$$T_b = \frac{1}{2}\rho A \int_0^{L_b} \{(\dot{y}_b + \dot{v})^2 + \dot{w}^2\}\,\mathrm{d}x, \tag{4}$$

$$\mathscr{T}_c = \frac{1}{2} m_c \{\dot{x}_c^2 + (\dot{y}_b + \dot{v}(x_c, t))^2 + \dot{w}(x_c, t)^2\} \tag{5}$$

and, after the substitutions $\cos\theta_x = C_{\theta_x}$, $\sin\theta_x = S_{\theta_x}$, $\cos\theta_y = C_{\theta_y}$ and $\sin\theta_y = S_{\theta_y}$,

$$\mathscr{T}_p = \frac{1}{2} m_p \{\dot{x}_x^2 + \dot{y}_b^2 + L_p^2 C_{\theta_x}^2 \dot{\theta}_y^2 + 2L_p \dot{x}_c C_{\theta_x} \dot{\theta}_x + \dot{v}^2(x_c, t) + \dot{w}^2(x_c, t) + 2\dot{y}_b \dot{v}(x_c, t)$$

$$+ 2L_p[(\dot{v}(x_c, t) + \dot{y}_b)(C_{\theta_x} C_{\theta_y} \dot{\theta}_y - S_{\theta_x} S_{\theta_y} \dot{\theta}_x) - \dot{w}(x_c, t)(C_{\theta_x} S_{\theta_y} \dot{\theta}_y + S_{\theta_x} C_{\theta_y} \dot{\theta}_x]\}. \tag{6}$$

The system total potential energy $\mathscr{U}$ is

$$\mathscr{U} = \frac{1}{2}\int_0^{L_b} \left[EI_{zz}\left(\frac{\partial^2 v}{\partial x^2}\right)^2 + EI_{yy}\left(\frac{\partial^2 w}{\partial x^2}\right)^2 \right] \mathrm{d}x - (m_c + m_p) g w(x_c, t) - \mathrm{m}_p \mathrm{g} \mathrm{L}_p \mathrm{C}_{\theta_x} \mathrm{C}_{\theta_y}. \tag{7}$$

The first two terms are the beam strain energy and the last two are the gravitational potential energy (g is the acceleration due to gravity) of the carriage and payload. It is expedient to introduce the following non-dimensional parameters:

$$\xi \triangleq \frac{x}{L_b}, \quad \xi_c \triangleq \frac{x_c}{L_b}, \quad l_p \triangleq \frac{L_p}{L_b}, \quad M_c \triangleq \frac{m_c}{\rho A L_b}, \quad \lambda_i^4 \triangleq \frac{\rho A L_b^4 w_i^2}{EI_{yy}},$$

$$\eta_b \triangleq \frac{y_b}{L_b}, \quad M_p \triangleq \frac{m_p}{\rho A L_b}, \quad M_{cp} \triangleq M_c + M_p, \quad \gamma_i^4 \triangleq \frac{\rho A L_b^4 w_i^2}{EI_{zz}} \tag{8}$$

and the dimensional ratio $\Omega^2 \triangleq g/L_b$.

As per the Rayleigh–Ritz solution technique and using the non-dimensional co-ordinate ξ, the elastic displacements are assumed such that

$$v(x, t) = L_b \mathbf{V}^{\mathrm{T}}(\xi)\mathbf{p}(t) \quad \text{and} \quad w(x, t) = L_b \mathbf{W}^{\mathrm{T}}(\xi)\mathbf{q}(t), \tag{9}$$

where $\mathbf{p}(t) = [p_1(t)\ p_2(t) \cdots p_n(t)]^{\mathrm{T}}$ and $\mathbf{q}(t) = [q_1(t)\ q_2(t) \cdots q_n(t)]^{\mathrm{T}}$ are column vectors of undetermined coefficients and $\mathbf{V}(\xi) = [V_1(\xi)\ V_2(\xi) \cdots V_n(\xi)]^{\mathrm{T}}$ and $\mathbf{W}(\xi) = [W_1(\xi)\ W_2(\xi) \cdots W_n(\xi)]^{\mathrm{T}}$ are column vectors of basis functions which in this case are the orthonormal eigenfunctions of a simply supported beam. Specifically,

$$V_i(\xi) = \sqrt{2}\sin(\gamma_i \xi) \quad \text{and} \quad W_i(\xi) = \sqrt{2}\sin(\lambda_i \xi),$$

where γ_i and λ_i are the non-dimensional circular eigenfrequencies of the the ith out-of-plane and in-plane modes respectively. Upon using the equations (8) and (9) as well as expressions (4)–(7) the Rayleigh–Ritz method yields the following equations of motion:

$$(\mathbf{I} + M_{cp}\mathbf{V}(\xi_c)\mathbf{V}(\xi_c)^{\mathrm{T}})\ddot{\mathbf{p}} + 2M_{cp}\dot{\xi}_c\mathbf{V}(\xi_c)\mathbf{V}'(\xi_c)^{\mathrm{T}}\dot{\mathbf{p}} + \left[M_{cp}(\ddot{\xi}_c\mathbf{V}(\xi_c)\mathbf{V}'(\xi_c)^{\mathrm{T}} + \dot{\xi}_c^2\mathbf{V}(\xi_c)\mathbf{V}''(\xi_c)^{\mathrm{T}}) + \frac{EI_{zz}\gamma_i^4}{\rho AL_b^4}\mathbf{I}\right]\mathbf{p} + \ddot{\eta}_b\left[M_{cp}\mathbf{V}(\xi_c) + \int_0^1 \mathbf{V}(\xi)\,\mathrm{d}\xi\right] + M_p l_p \mathbf{V}(\xi_c)\ddot{\theta}_y = 0, \tag{10}$$

$$(\mathbf{I} + M_{cp}\mathbf{W}(\xi_c)\mathbf{W}(\xi_c)^{\mathrm{T}})\ddot{\mathbf{q}} + 2M_{cp}\dot{\xi}_c\mathbf{W}(\xi_c)\mathbf{W}'(\xi_c)^{\mathrm{T}}\dot{\mathbf{q}} + \left[M_{cp}(\ddot{\xi}_c\mathbf{W}(\xi_c)\mathbf{W}'(\xi_c)^{\mathrm{T}} + \dot{\xi}_c^2\mathbf{W}(\xi_c)\mathbf{W}''(\xi_c)^{\mathrm{T}}) + \frac{EI_{yy}\lambda_i^4}{\rho AL_b^4}\mathbf{I}\right]\mathbf{q} - \Omega^2 M_{cp}\mathbf{W}(\xi_c) = 0, \tag{11}$$

$$l_p\ddot{\theta}_x + [\Omega^2 - \mathbf{W}(\xi_c)^{\mathrm{T}}\ddot{\mathbf{q}} - 2\dot{\xi}_c\mathbf{W}'(\xi_c)^{\mathrm{T}}\dot{\mathbf{q}} - (\ddot{\xi}_c\mathbf{W}'(\xi_c)^{\mathrm{T}} + \dot{\xi}_c^2\mathbf{W}''(\xi_c)^{\mathrm{T}})\mathbf{q}]\,\theta_x + \ddot{\xi}_c = 0, \tag{12}$$

$$l_p\ddot{\theta}_y + [\Omega^2 - \mathbf{W}(\xi_c)^{\mathrm{T}}\ddot{\mathbf{q}} - 2\dot{\xi}_c\mathbf{W}'(\xi_c)^{\mathrm{T}}\dot{\mathbf{q}} - (\ddot{\xi}_c\mathbf{W}'(\xi_c)^{\mathrm{T}} + \dot{\xi}_c^2\mathbf{W}''(\xi_c)^{\mathrm{T}})\mathbf{q}]\,\theta_y + [\mathbf{V}(\xi_c)^{\mathrm{T}}\ddot{\mathbf{p}} + 2\dot{\xi}_c\mathbf{V}'(\xi_c)^{\mathrm{T}}\dot{\mathbf{p}} + (\ddot{\xi}_c\mathbf{V}'(\xi_c)^{\mathrm{T}} + \dot{\xi}_c^2\mathbf{V}''(\xi_c)^{\mathrm{T}})\mathbf{p}] + \ddot{\eta}_b = 0, \tag{13}$$

where $\mathbf{I}$ is an identity matrix.

Equations (10)–(13) call for a few remarks. First, the in-plane beam motion w uncouples from the other motions (i.e., the out-of-plane motion v, and the payload motions θ_x and θ_y) but not conversely. Second, the in-plane motion w behaves as a stiffness modulator in the payload motions θ_x and θ_y (see equations (12) and (13)) and has the potential to make the motion unstable because equation (12) has the Hill–Mathieu form. Third, with reference to equations (10) and (13), the out-of-plane motion v does not uncouple from the payload out-of-plane motion θ_y; they act as forcing terms on each other. Fourth, the travel of the beam η_b is only manifest as a forcing term in the out-of-plane motions (equations (10) and (13)) where it appears as an acceleration. Fifth, while the in-plane motion (11) is invariant to the individual carriage and payload masses for a given constant sum of carriage mass and payload mass m_{cp}, the out-of-plane deflection (10) is explicitly dependent on the payload mass through the coupling with the out-of-plane payload motion. Finally, the equations are non-linear in the carriage speed $\dot{\xi}_c$.

It is important to include the non-linear contribution of the traverse speed since, in the engineering design sense, the linear analysis is non-conservative when the carriage speed is sufficiently large, i.e., the linear analysis yields beam deflections that are smaller than those obtained with the non-linear analysis. Thus, the non-linearity is retained in the numerical simulations presented in the next section of the paper.

For beam travel alone (i.e., ξ_c = constant), equations (10)–(13) become

$$(\mathbf{I} + M_{cp}\mathbf{V}(\xi_c)\mathbf{V}(\xi_c)^{\mathrm{T}})\ddot{\mathbf{p}} + \frac{EI_{zz}\gamma_i^4}{\rho AL_b^4}\mathbf{p} + \ddot{\eta}_b\left[M_{cp}\mathbf{V}(\xi_c) + \int_0^1 \mathbf{V}(\xi)\,\mathrm{d}\xi\right] + M_p l_p \mathbf{V}(\xi_c)\ddot{\theta}_y = 0, \tag{14}$$

$$(\mathbf{I} + M_{cp}\mathbf{W}(\xi_c)\mathbf{W}(\xi_c)^{\mathrm{T}})\ddot{\mathbf{q}} + \left[\frac{EI_{yy}\lambda_i^4}{\rho AL_b^4}\mathbf{I}\right]\mathbf{q} - \Omega^2 M_{cp}\mathbf{W}(\xi_c) = 0, \tag{15}$$

$$l_p\ddot{\theta}_x + [\Omega^2 - \mathbf{W}(\xi_c)^{\mathrm{T}}\ddot{\mathbf{q}}]\theta_x = 0, \tag{16}$$

$$l_p\ddot{\theta}_y + [\Omega^2 - \mathbf{W}(\xi_c)^{\mathrm{T}}\ddot{\mathbf{q}}]\theta_y + [\mathbf{V}(\xi_c)^{\mathrm{T}}\ddot{\mathbf{p}}] + \ddot{\eta}_b = 0. \tag{17}$$

It is worth noting that if the beam were rigid then the angle of the pendulum (θ) in the direction transverse to the pivot motion would be given by the solution of

$$l_p\ddot{\theta} + \Omega^2\theta = 0 \tag{18}$$

and the angle in the direction of the pivot motion ($\zeta(t)$) would be governed by

$$l_p\ddot{\theta} + \Omega^2\theta + \ddot{\zeta} = 0. \tag{19}$$

4. NUMERICAL EXAMPLES AND COMMENTS

The beam used in the following numerical examples has the properties given in Table 1. This choice of parameters has been selected, in the first instance, to facilitate a comparison between the present results and those obtained by Pesterev and Bergman [6, 7]. The time required for both carriage traverse and beam travel has been fixed at 60 s in agreement with the examples used by Pesterev and Bergman [6, 7]. It is apparent from the equations derived above that the acceleration and deceleration phases are the most significant and changing the time duration of the simulation, keeping all other parameters constant, would either diminish the period of constant velocity or extend it. Keeping the constant velocity duration unchanged would require larger accelerations (shorter overall times) or smaller accelerations (longer overall times). The issue of motion trajectory is more suitably dealt with as a control problem and it has not been treated as a parameter that will be varied in the following examples.

Pesterev and Bergman [6, 7] considered three cases, each distinguished by a different carriage traversal motion but with no beam travel. In the first case, the carriage traversed the beam with a constant speed, in the second case, the carriage decelerated uniformly from an initial speed of 12 to 0 m/s and in the third case, the carriage accelerated uniformly from an initial speed of 0 m/s. Excellent agreement was found between the example results reported in references [6, 7] and the results found by repeating those examples with the model developed above.

The payload swing is affected by the carriage traverse and beam travel accelerations, $\ddot{x}_c$ and $\ddot{y}_b$ respectively. In practice, the carriage (or beam) starts with a zero initial velocity, accelerates to a particular speed which could be held constant for some time before decelerating to rest. All the following cases are based on traversal or travel profiles

TABLE 1

Beam property values

E	$2{\cdot}11 \times 10^{11}$ Nm^2	v	0·33
L_b	6 m	A	$20{\cdot}396 \times 10^{-3}$ m^2
I_{yy}	$2{\cdot}13 \times 10^{-7}$ m^4	I_{zz}	$2{\cdot}13 \times 10^{-7}$ m^4
ρ	$8{\cdot}0 \times 10^3$ kg/m^3	g	9.81 m/s
M_c	0	M_c	0·1
ω_{b1}	0·724 Hz	ω_{b1}	0·6609 Hz
ω_{b2}	2·897 Hz	ω_{b2}	2·897 Hz

represented by a quintic polynomial which allows for a smooth transition between the different motions. The overall motion is divided into three time intervals, $[0, t_1]$, $[t_1, t_2]$, and $[t_2, t_f]$. The duration of the simulation is t_f, t_1 denotes the end of the acceleration interval, the interval $[t_1, t_2]$ is the period of constant speed and the final interval is deceleration. In all cases, the terminal times of the intervals are $t_1 = 15$ s, $t_2 = 45$ s and $t_f = 60$ s and the displacement at the end of the first interval is 1 m, the speed during the constant speed phase is 0·133 m s^{-1} and the deceleration phase occurs over the last meter of the motion. The initial displacements for each swing angle are $\theta_x(0) = -0{\cdot}01$ and $\theta_y(0) = -0{\cdot}01$. Although the governing equations of motion are non-linear and an FFT analysis of the signals is not strictly appropriate it has been used in each of the following cases to obtain an estimate of the frequency content of each simulation to allow comparison.

4.1. CASE 1: EFFECT OF PENDULUM LENGTH

In the following simulations the pendulum length is varied while keeping the travel and traverse profiles as described above.

4.1.1. *Beam travel*

For beam travel alone (i.e., no traverse motion and with $\xi_c = 0{\cdot}5$) the governing equations are equations (14)–(17). The non-dimensional masses and lengths of the beam–carriage–payload system are given in Table 2. The swing angles θ_x and θ_y, as obtained by numerically solving equations (14)–(17), are depicted in Figures 2 and 3 respectively. If the beam were rigid, θ_x would be expected to behave as a simple harmonic oscillator as predicted by equation (18) and θ_y would be consistent with equation (19). The difference between the closed-form results obtained from equations (18) and (19), and those obtained from the numerical solution of equations (14)–(17) are shown in Figures 4 and 5 where $\Delta\theta = \theta_{\text{flexible}} - \theta_{\text{rigid}}$. It may be observed, by comparing Figures 2 and 4 that for $l_p = \frac{1}{3}$, $\Delta\theta_x > \theta_x$; a result which at first glance seems counter-intuitive. It may be understood by considering Figure 6 where it may be observed that the θ_x trajectories have different frequencies; an FFT analysis of the data in this figure shows that the dominant frequency in the rigid beam case is 0·358 Hz and in the flexible beam case is 0·342 Hz. Signals with these frequencies will be out of phase at approximately $t = 51{\cdot}3$ s, which is what may be observed in the figure. The acceleration and deceleration phases are not as apparent in Figure 3 as they are in Figure 7 because in the former case, the forcing term is no longer solely dependent on the travel acceleration.

Recall that Figures 2 and 4 are for a motion that is transverse to the travel of the beam and it could be reasonably expected that the difference between the results for the rigid- and the flexible-beam assumption would be negligible. It is found that the difference is actually relatively large, on the same order of magnitude as the initial angular displacement for θ_x. This behaviour is entirely due to the flexibility of the beam as shown in equation (16) where it may be seen that θ_x couples to $\ddot{w}$ which in turn is governed by the uncoupled linear ordinary differential equation (15) ($\dot{\xi}_c = 0$ and $\ddot{\xi}_c = 0$) that predicts a periodic behaviour of $w(x, t)$. The frequencies present in $w(x, t)$ are given by the eigenvalues of the simplified form of equation (15) and are approximations to the natural frequencies of the beam/carriage/payload system. The first two natural frequencies, as determined by the analytical frequency equation [10], are given in Table 2. These values are identical to the eigenvalues. The periodicity of $w(x, t)$ manifests itself in equations (16) by contributing a time-varying

TABLE 2

Parameter and result values for the pendulum length effect examples

M_p	0·05				0·1				0·15		0·25	
ω_{b1} (Hz)	0·635				0·612				0·591		0·555	
ω_{b2} (Hz)	2·897				2·897				2·897		2·897	
l_p	$\frac{2}{3}$		$\frac{1}{3}$		$\frac{2}{3}$		1		$\frac{2}{3}$		$\frac{2}{3}$	
ω_p (Hz)	0·249		0·352		0·249		0·204		0·249		0·249	
Beam travel motion												
	θ_x	θ_y	θ_x	θ_y	θ_x	θ_y	θ_x	θ_y	θ_x	θ_y	θ_x	θ_y
$\hat{\omega}_1$ (Hz)	0·244	0·244	0·342	0·326	0·244	0·244	0·212	0·195	0·260	0·244	0·260	0·244
$\hat{\omega}_2$ (Hz)	0·374	0·374	0·260	0·277	0·358	0·358	0·407	0·407	0·326	0·342	0·293	0·309
Carriage traverse motion												
$\hat{\omega}_1$ (Hz)	0·244	0·244	0·358	0·342	0·244	0·244	0·212	0·195	0·244	0·244	0·244	0·277
$\hat{\omega}_2$ (Hz)	—	—	—	—	—	—	—	—	—	—	—	0·212

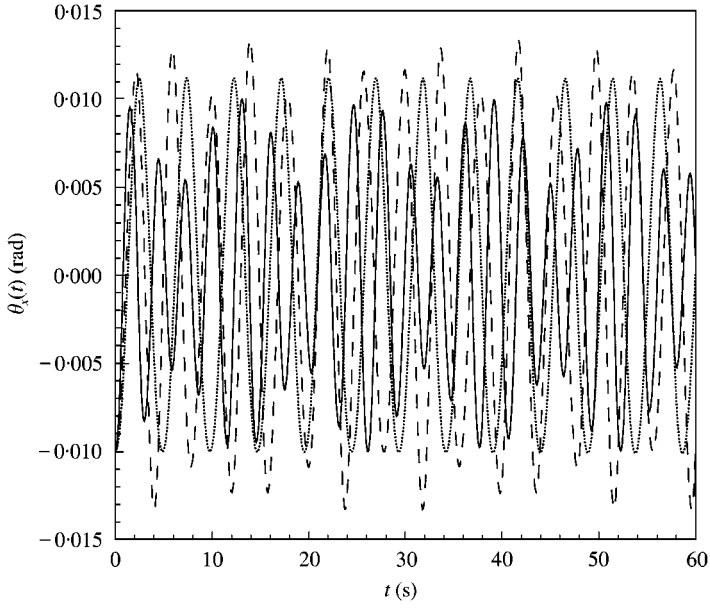

Figure 2. Effect of pendulum length on in-plane swing, beam travel motion: (——) $l_p = \frac{1}{3}$; (— — —) $l_p = \frac{2}{3}$; (· · · · · ·) $l_p = 1$.

component to the frequency coefficient of θ_x. This explains why, in Figure 4, the difference increases with time with the rate of increase being such that the peak amplitude of $\Delta\theta_x$ increases faster for $l_p = \frac{1}{3}$ than for $l_p = \frac{2}{3}$ which increases faster than for $l_p = 1$. For the short pendulum ($l_p = \frac{1}{3}$) the amplitude of θ_x is always less than its initial magnitude (see Figure 2). When $l_p = \frac{2}{3}$ the amplitude of θ_x regularly exceeds the initial magnitude but the $l_p = 1$ pendulum exhibits oscillations that are greater than those for $l_p = \frac{1}{3}$ but less than those for $l_p = \frac{2}{3}$.

With reference to the responses shown in Figures 2 and 3 the first of the two most dominant frequencies $\hat{\omega}_1$ and $\hat{\omega}_2$, as determined from an FFT analysis, decreases with increasing length of pendulum while the second dominant frequency increases (see Table 2).

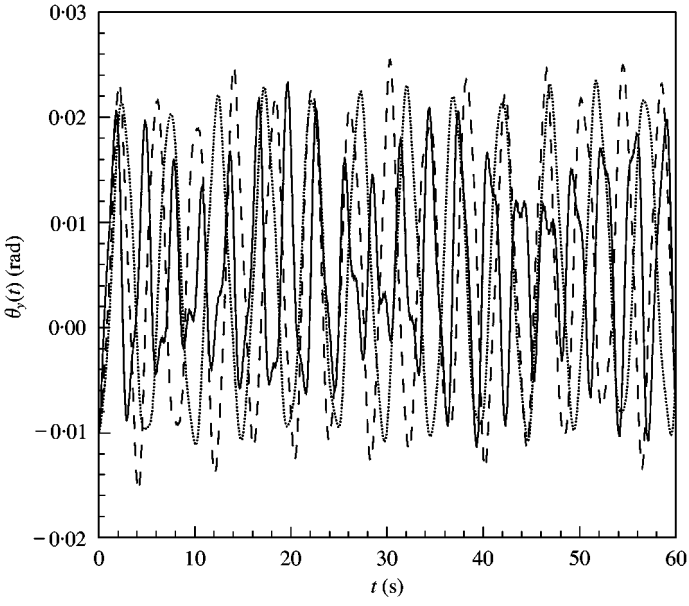

Figure 3. Effect of pendulum length on out-of-plane swing, beam travel motion: (——) $l_p = \frac{1}{3}$; (— — —) $l_p = \frac{2}{3}$; (·····) $l_p = 1$.

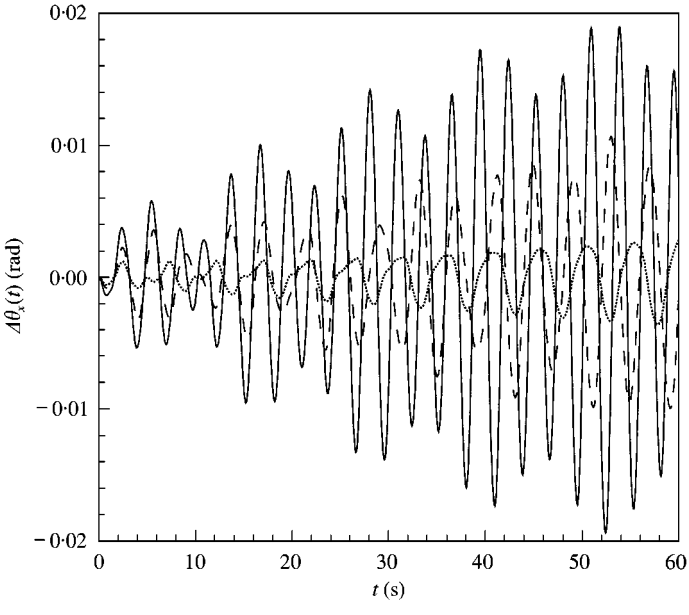

Figure 4. Rigid/flexible difference of in-plane swing, beam travel motion: (——) $l_p = \frac{1}{3}$; (— — —) $l_p = \frac{2}{3}$; (·····) $l_p = 1$.

Further, with reference to Table 2, both the in-plane and out-of-plane swing results show that for all but the $l_p = 1$, θ_x case the dominant frequency is lower than the pendulum's natural frequency. The frequency step size (0·016 Hz) used in the FFT analysis is responsible for the apparent discrepancy in the $l_p = 1$ case.

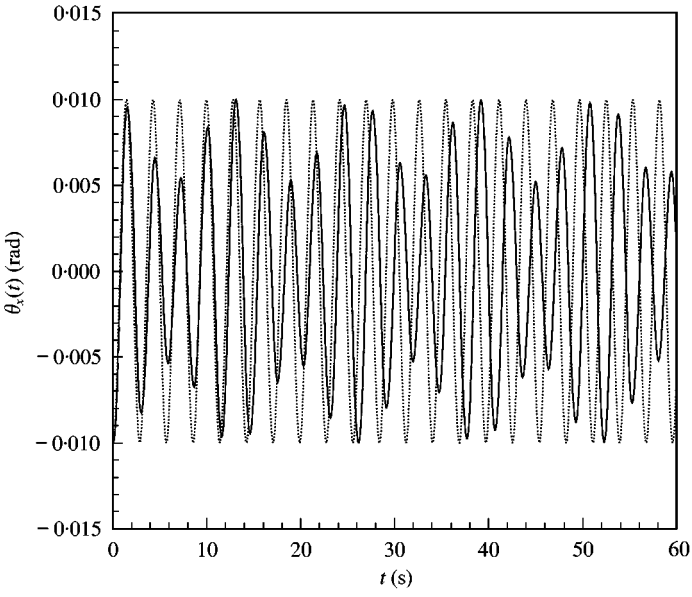

Figure 5. Rigid and flexible beam in-plane swing responses, beam travel motion: (——) flexible beam; (— — —) rigid beam; $l_p = 1/3$.

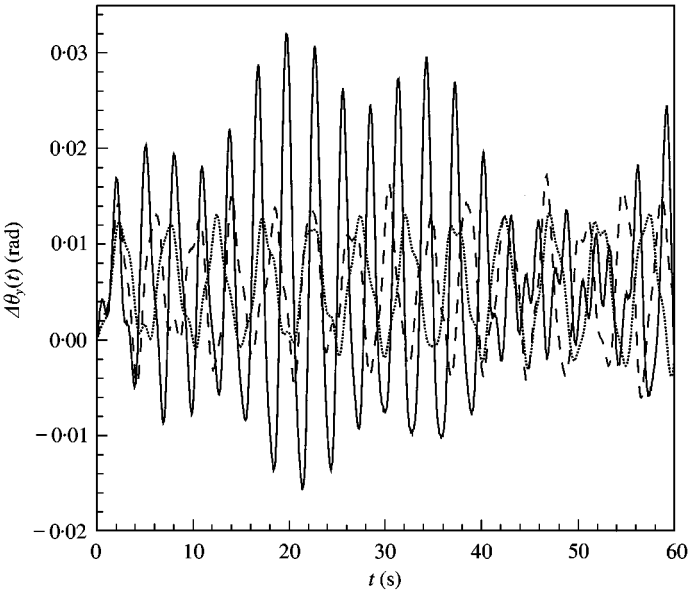

Figure 6. Rigid/flexible difference of out-of-plane swing, beam travel motion: (——) $l_p = \frac{1}{3}$; (— — —) $l_p = \frac{2}{3}$; (·····) $l_p = 1$.

The amplitude of θ_y (Figure 3) exceeds the initial amplitude for all pendulum lengths investigated and has a positive mean value due the energy added to the pendulum during the acceleration phase of the motion. Additionally, the forcing term is no longer solely dependent on the travel acceleration. Given the positive deviations, one can conclude that the contribution due to elasticity $V(\xi_c)^{\mathrm{T}}\ddot{p}$ is dominating the acceleration contribution. In the

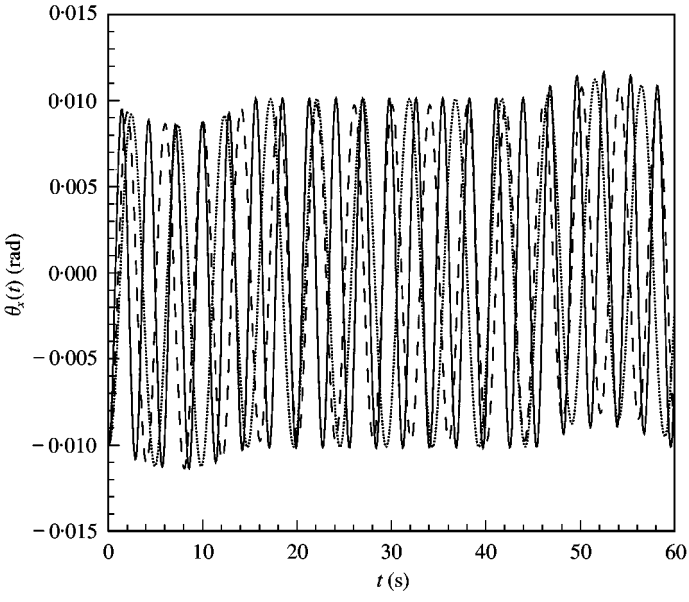

Figure 7. Effect of pendulum length on in-plane swing, carriage traverse motion: (——) $l_p = \frac{1}{3}$; (— — —) $l_p = \frac{2}{3}$; (.....) $l_p = 1$.

$l_p = \frac{1}{3}$ case there is clear evidence of higher order frequency components in the response. The difference between the response of θ_y for the rigid- and flexible-beam models is illustrated in Figure 6 were it may be observed that the largest difference corresponds to the pendulum of shortest length and that for that pendulum there is a distinctive beat-like behavior.

4.1.2. *Carriage traversal*

The results for θ_x and θ_y for the case of the carriage traversal (no beam travel, $\ddot{\eta}_b = 0$) are illustrated in Figures 7 and 8 respectively. As in the beam travel case discussed previously, if the beam were rigid θ_y would be expected to behave as a simple harmonic oscillator as predicted by equation (18) and θ_x would be consistent with equation (19). The difference between the results obtained from equations (18) and (19) and those obtained from the numerical solution of equations (14)–(17) are shown in Figures 9 and 10.

In Figure 7, it is easy to identify the end of the acceleration phase ($t = 15$ s) and the beginning of the deceleration phase ($t = 45$ s) in the response of θ_x. During those portions of the carriage motion, θ_x exhibits small excursions beyond its initial value and during the constant speed phase of the motion, θ_x behaves in a stable periodic fashion that contrasts quite strongly with the motion described by θ_y in the beam travel case (Figure 3) discussed above. The acceleration and deceleration phases are more apparent in Figure 7 than they are in Figure 3 because in the latter case, the forcing term is not solely dependent on the travel acceleration, as it is here. This difference must be due to the non-linear contributions from $\dot{\xi}_c$ and $\ddot{\xi}_c$ in the governing equations (10)–(13); non-linearities that are not present in equations (14)–(17).

A further difference between the beam travel and the carriage traverse cases can be appreciated by observing in Figure 9 that the difference between the rigid-beam assumption and the flexible-beam model results is, in the carriage traverse case, negligible. The clear beating behaviour illustrated in Figure 9 is of interest.

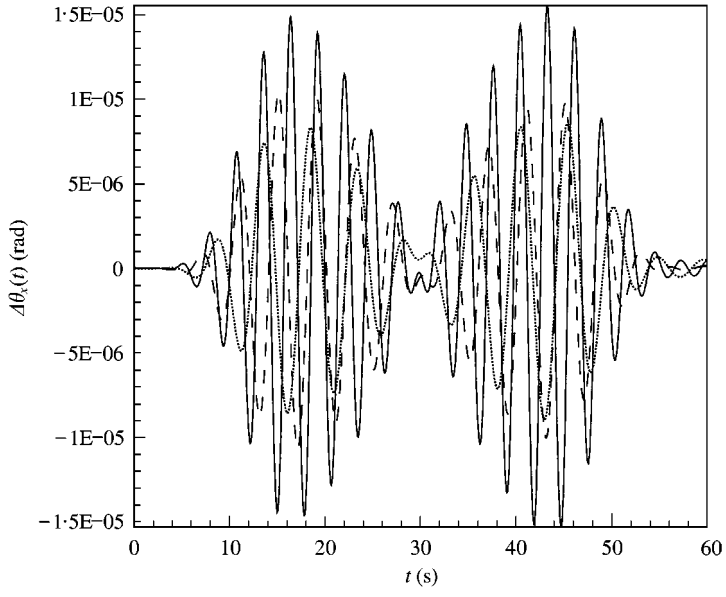

Figure 8. Rigid/flexible difference of in-plane swing, carriage traverse motion: (——) $l_p = \frac{1}{3}$; (— — —) $l_p = \frac{2}{3}$; (.....) $l_p = 1$.

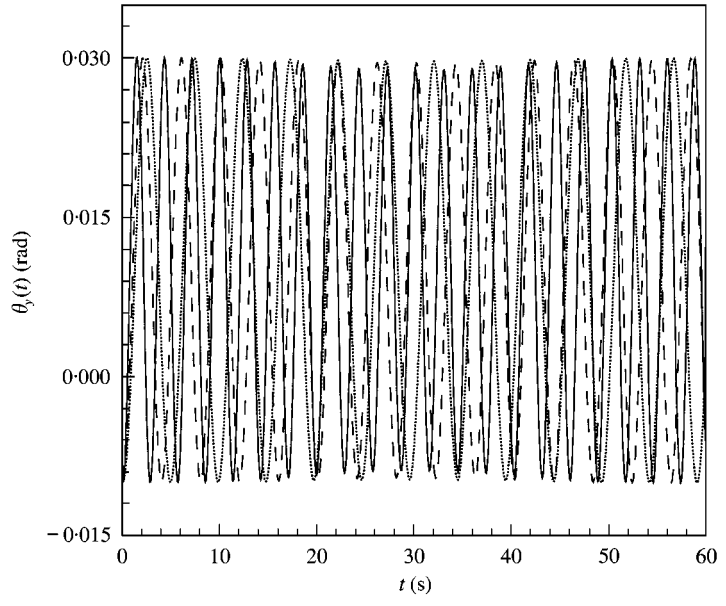

Figure 9. Effect of pendulum length on out-of-plane swing, carriage traverse motion: (——) $l_p = \frac{1}{3}$; (— — —) $l_p = \frac{2}{3}$; (.....) $l_p = 1$.

Unlike θ_x, θ_y uniformly exceeds its initial amplitude but only in the positive direction and quite uniformly by a factor of close to three. This accounts for the large $\Delta\theta_y$ values in Figure 10. The growth in $\Delta\theta_y$ for the $l_p = \frac{1}{3}$ case during approximately the last 2/3rds of the time history is unexplained except to observe that the same behavior, but to a far lesser degree, occurs for the other two cases as well.

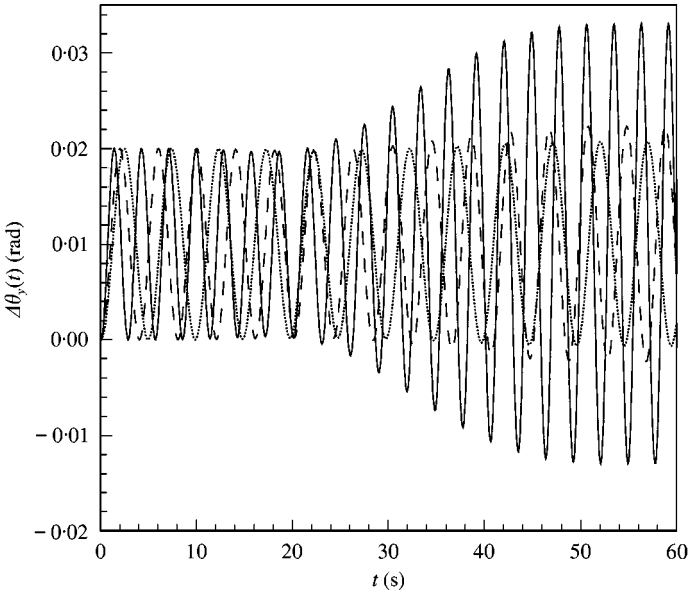

Figure 10. Rigid/flexible difference of out-of-plane swing, carriage traverse motion: (——) $l_p = \frac{1}{3}$; (— — —) $l_p = \frac{2}{3}$; (·····) $l_p = 1$.

4.2. CASE 2: EFFECT OF PAYLOAD MASS

For a simple pendulum, with or without a moving pivot, the mass of the pendulum does not contribute to the dynamics of the system. The addition of the flexible beam changes that. Equation (10) depends on the combined carriage/payload mass M_{cp} and the payload mass M_p but equation (11) directly depends only on the sum M_{cp}. Neither θ_x nor θ_y, equations (12), (13), explicitly depend on either M_p or M_{cp}. The effect of payload mass is examined by fixing the non-dimensional pendulum length at $l_p = \frac{2}{3}$, the non-dimensional carriage mass at $M_c = 0{\cdot}1$, and the non-dimensional payload mass $M_p \in \{0{\cdot}05, 0{\cdot}15, 0{\cdot}25\}$.

4.2.1. *Beam travel*

The angles θ_x and θ_y, for each value of M_p and with the beam in travel motion ($\xi_c = \text{constant} = 0{\cdot}5$), are plotted in Figures 11 and 12 respectively. The role that the payload mass plays in the swing response is very evident in these two figures where it may be seen that the peak amplitudes increase with increasing mass and are much greater than the amplitude increases due to increasing pendulum length. Additionally, just as in Figure 3, the forcing term is no longer solely dependent on the travel acceleration. The positive deviations are due to the elasticity contribution $V(\xi_c)^{\mathrm{T}}\ddot{p}$ which is dominating the acceleration contribution. The acceleration and deceleration phases are not as apparent in Figure 12 as they are in Figure 13 because in the former case, the forcing term is no longer solely dependent on the travel acceleration.

In the $l_p = \frac{1}{3}$ case there is clear evidence of higher order frequency components in the response. The difference between the response of θ_y for the rigid- and flexible-beam models is illustrated in Figure 6 were it may be observed that the greatest difference corresponds to the pendulum of shortest length and that for that pendulum there is a distinctive beat-like behavior.

The frequency content of these results, as obtained from an FFT analysis, are reported in Table 2. The frequencies associated with the larger masses are higher than the pendulum

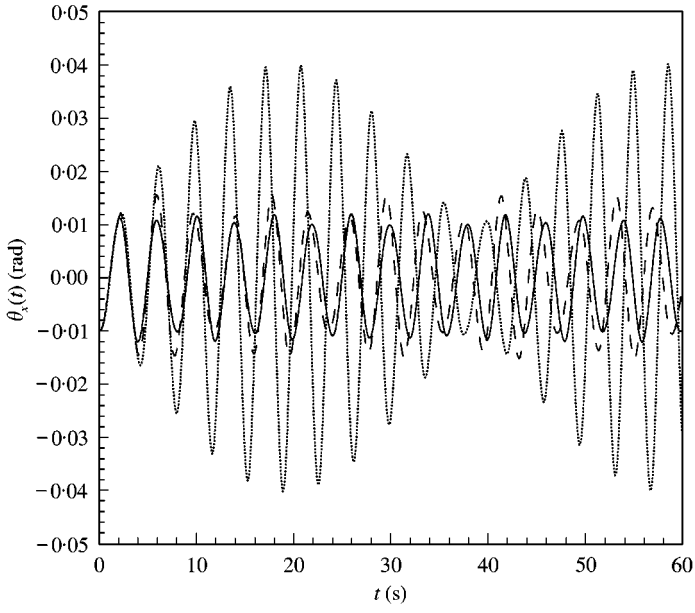

Figure 11. Effect of payload mass on in-plane swing, beam travel motion: (——) $M_p = 0{\cdot}05$; ; (— — —) $M_p = 0{\cdot}10$; (·····) $M_p = 0{\cdot}15$.

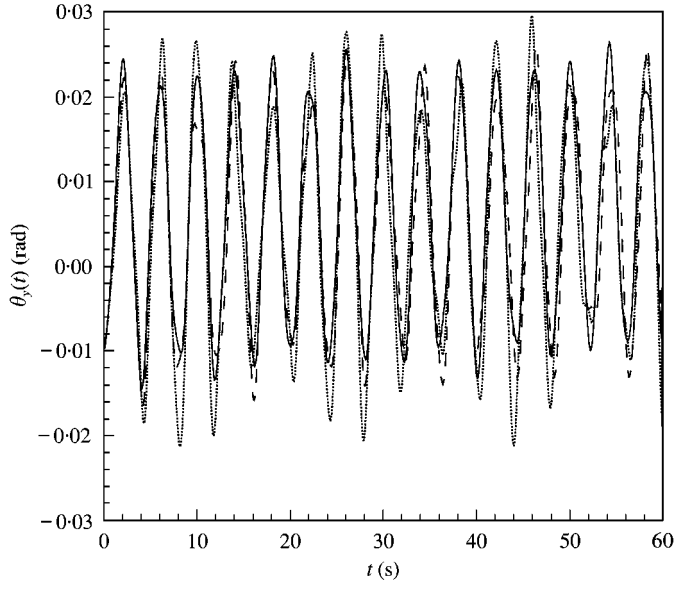

Figure 12. Effect of payload mass on out-of-plane swing, beam travel motion: (——) $M_p = 0{\cdot}05$; (— — —) $M_p = 0{\cdot}10$; (·····) $M_p = 0{\cdot}15$.

natural frequency of 0·249 Hz. As in the pendulum length examples the differences between the results, assuming a rigid and a flexible beam, are large.

4.2.2. *Carriage traverse*

The corresponding results for the carriage traverse motion (no travel, $\eta = 0$) are depicted in Figures 13–15. The results for θ_x and θ_y during the carriage traverse motion show that θ_x

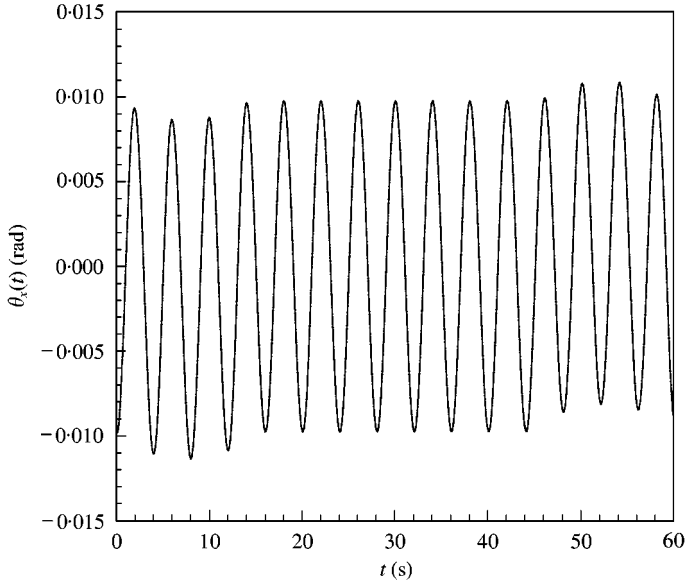

Figure 13. Effect of payload mass on in-plane swing, carriage traverse motion: (——) $M_p = 0{\cdot}05$; (— — —) $M_p = 0{\cdot}10$; (.....) $M_p = 0{\cdot}15$.

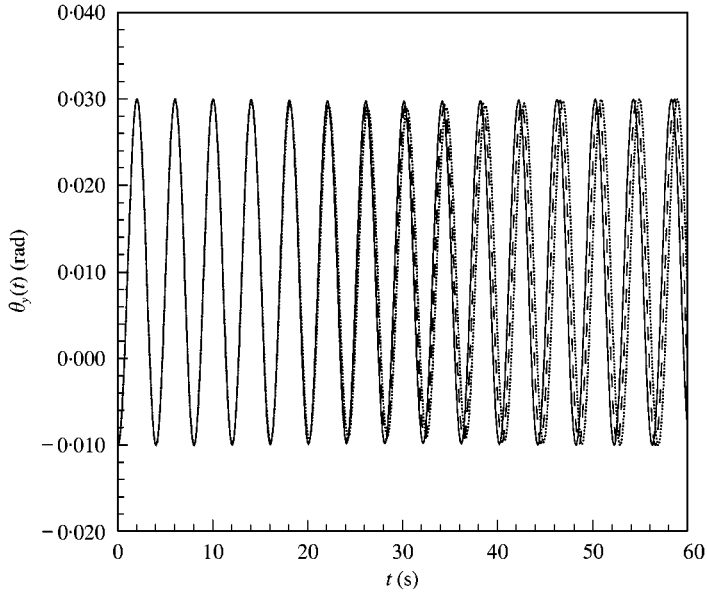

Figure 14. Effect of payload mass on out-of-plane swing, carriage traverse motion: (——) $M_p = 0{\cdot}05$; (— — —) $M_p = 0{\cdot}10$; (.....) $M_p = 0{\cdot}15$.

(Figure 13) has a single frequency component at $\hat{\omega}_1 = 0{\cdot}244$ Hz. Figure 13 also shows that the payload mass has no effect on the θ_x response in this case. The effect of the acceleration and deceleration phases can be clearly seen in this figure. An examination of the difference between the rigid- and flexible-beam results shows that the in-plane swing θ_x deviates only minutely between the two cases; θ_x behaves very much as if the beam were rigid for carriage

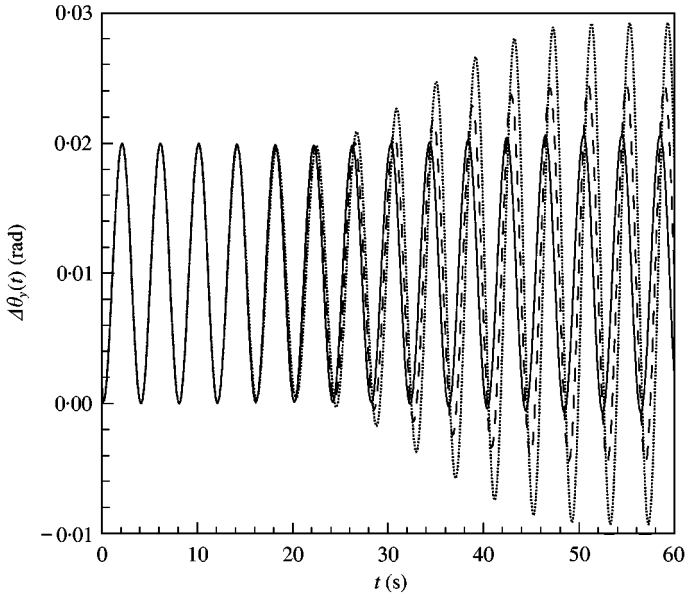

Figure 15. Rigid/flexible difference of out-of-plane swing, carriage traverse motion: (——) $M_p = 0{\cdot}05$; (— — —) $M_p = 0{\cdot}10$; (.....) $M_p = 0{\cdot}15$.

traverse motion. The plotted result appears very much as the results which appear in Figure 9.

Both the θ_x and θ_y signals (Figures 14 and 15) have a single dominant frequency of $\hat{\omega}_1 = 0{\cdot}244$ Hz except in the case of θ_y when $M_p = 0{\cdot}25$. Figure 15 shows that θ_y does not behave in a manner which is close to the calculated rigid-beam response. There is an interesting similarity between Figures 10 and 15; both show instances where there is a significant divergence from the rigid-beam behavior. In Figure 10, this occurs for the shortest pendulum and in Figure 15 it occurs for the heaviest pendulum. The acceleration and deceleration phases are more apparent in Figure 13 than they are in 12 because in the latter case, the forcing term is not solely dependent on the travel acceleration, as it is here.

5. SUMMARY

The system assumptions yield equations of motion where the vertical vibration of the beam couples with the other motions, but not conversely. The in-plane beam deformation appears as a stiffness modulator in the equations for the θ_x and θ_y motions. The θ_y motion and beam displacement $v(x, t)$ couple with each other as forcing terms. Hence, the vertical beam motion implicitly couples with the horizontal beam motion. Further, it is observed that the traverse and travel accelerations act as forcing terms in the θ_x and θ_y swing motions respectively. The effect of the beam travel motion is neither manifested in the θ_x motion as a velocity term nor as an acceleration term. This, however, cannot be said for the effect of carriage motion over a fixed beam on the θ_y motions. The examples indicate that the swing angles and frequencies are dependent on the length of the pendulum and the payload mass or the combined payload and carriage mass. The pendulum length results show that the dominant frequencies in the swing responses decreased with increasing pendulum length.

The amplitude of swing angle increased with increasing payload mass, because of the increasing contributions of the forcing terms. Minimal changes were observed in the swing angle frequencies for corresponding changes in payload mass. This analysis reveals the complexity of the three-dimensional overhead crane dynamics. Further assumptions or approximations may be necessary to have a simpler, yet valid, model that will effectively represent the system dynamics. Presently, it may be worthwhile to adopt a problem specific approach to the design and control issues.

REFERENCES

1. A. R. GOLAFSHANI and J. D. APLEVICH 1995 *Proceedings of the* 4*th IEEE Conference on Control Applications*, *Albany*, *NY*, 28–29 September. 1134–1139. Computation of time-optimal trajectories for tower cranes.
2. A. R. GOLAFSHANI and J. D. APLEVICH 1995 *Proceedings of the* 3*rd SIAM Conference on Control and its Applications, St. Louis, April* 27–29. Time-optimal control of basic motion of tower cranes.
3. L. FRYBA 1972 *Vibrations of Solids and Structures Under Moving Loads*. Groningen: Noordhoff.
4. M. M. STANISIC 1985 *Ingenieur-Archiv* **55**, 176–185. On a new theory of the dynamic behaviour of the structures carrying moving masses.
5. S. SADIKU and H. H. E. LEIPHOLZ 1987 *Ingenieur-Archiv* **57**, 223–242. On the dynamics of elastic systems with moving masses.
6. A. V. PESTEREV and L. A. BERGMAN 1997 *American Society of Mechanical Engineers Journal of Engineering Mechanics* **123**, 878–884. Response of elastic continuum carrying moving linear oscillator.
7. A. V. PESTEREV and L. A. BERGMAN 1997 *American Society of Mechanical Engineers Journal of Engineering Mechanics* **123**, 886–889. Vibration of elastic continuum carrying accelerating oscillator.
8. M. OLSSON 1985 *Journal of Sound and Vibration* **99**, 1–12. Finite element, modal co-ordinate analysis of structures subjected to moving loads.
9. J. HINO, T. YOSHIMURA, K. KONISHI and N. A. ANANTHANARAYANA 1984 *Journal of Sound and Vibration* **96**, 45–53. Finite element method prediction of the vibration of a bridge subjected to a moving vehicle load.
10. D. C. D. OGUAMANAM, J. S. HANSEN and G. R. HEPPLER 1998 *Journal of Sound and Vibration* **213**, 889–906. Dynamic response of an overhead crane.
11. H.-H. LEE 1998 *American Society of Mechanical Engineers Journal of Dynamic Systems, Measurement, and Control* **120**, 471–476. Modeling and control of a three-dimensional overhead crane.